# Silver Nanowire Electrodes Integrated in Organic Solar Cells with Thick Active Layer Based on a Low-Cost Donor Polymer

Issoufou Ibrahim Zamkoye, Johann Bouclé, Nicolas Leclerc, Bruno Lucas, S Vedraine

# Silver Nanowire Electrodes Integrated in Organic Solar Cells with Thick Active Layer Based on a Low-Cost Donor Polymer

*Issoufou IBRAHIM ZAMKOYE, Johann BOUCLÉ, Nicolas LECLERC, Bruno LUCAS, and Sylvain VEDRAINE**

I. IBRAHIM ZAMKOYE, J. BOUCLÉ, B. LUCAS, S. VEDRAINE
Univ. Limoges, XLIM, UMR 7252, F-87000 Limoges, France
CNRS, XLIM, UMR 7252, F-87000 Limoges, France
E-mail: sylvain.vedraine@xlim.fr

N. LECLERC
Institut de Chimie et Procédés pour l'Energie, l'Environnement et la Santé (ICPEES), Université de Strasbourg, CNRS, UMR 7515, 25 rue Becquerel, 67087 Strasbourg, Cedex 02, France

**Abstract:**
Transparent electrodes are a key component in the manufacturing of optoelectronic devices such as LEDs, touch screens, and solar cells. The transparent electrode commonly used in this field is based on indium tin oxide (ITO). It contains indium, which is an expensive, rare, difficult to extract and depleting element, hence the need to find an alternative. Silver Nanowire (AgNW) electrodes are one of the best alternatives due to their excellent electrical, optical, and mechanical properties. In this work we show that embedding AgNWs between two layers of ZnO nanoparticles (ZnONPs) leads to superior optical and electrical performance. The validation of the ZnONPs /AgNWs/ ZnONPs (ZAZ) electrode using the reference PF2:PC70BM organic active layer, known to resent a long carrier lifetime, in inverted solar cell architectures shows an increased absorption of the active layer. This enhancement is due to the electrical field resulting from plasmonic resonance since the absorption is proportional to the square of the electric field amplitude. Through photoluminescence spectroscopy, we also observed a shorter exciton lifetime in PF2 in the presence of AgNWs. All these processes lead to improved photovoltaic performance compared to ITO-based reference, with approximately 20% increase in photocurrent and overall power conversion efficiency.

Keywords: Silver nanowires, transparent electrodes, organic solar cells, plasmonic resonance

## 1. Introduction

The photovoltaic industry is widely dominated by silicon-based solar cells. They account for more than half of the photovoltaic market share. [1] However, the manufacturing process of silicon-based solar cells is energy intensive due to its complexity. Which makes it costly to commercialize. Therefore, new technologies to make the manufacturing of solar cells low cost are increasingly being studied. In the last few years, organic solar cells have become very attractive to the research because of their advantages such as : low cost, flexibility, easily integrated, and non-toxic. [1,2] As a result, they have gone from less than 10% power conversion efficiency (PCE) in 2012 to 20% in 2022, [2-4] demonstrating the potential for production at the commercial scale. [1]

Due to the relatively low mobility (on order of $10^{-4}$ $cm^2/V.s$) of carriers and the short diffusion length in most organic semiconductors, [5], the active layer of OSCs is required to be thin in most cases, i.e., about 100nm or less. This feature allows facilitating the diffusion and extraction of charge carriers. [6] For several decades, the transparent electrode commonly used in this field is based on indium tin oxide (ITO) because of its high optoelectronic performances (transparency and conductivity). [7] However, the fabrication of ITO requires a vacuum and high temperature deposition technique. [8] Moreover, indium is a scarce material, hard to extract and especially disappearing, pushing towards the quest for alternatives. Silver nanowire based electrodes are a promising alternative because of their excellent optical, electrical and mechanical properties: transparency, conductivity and flexibility. [8] They have proven to be able to be used as an anode, cathode or interlayer of tandem organic solar cells. [9]

In addition, several studies show that the surface plasmon resonance related to metallic nanostructures can increase the absorption of the active layer. [8-9] The shape, size and chemical composition of these nanostructures are parameters that can be adapted to increase the influence of the plasmon resonance on the active layer absorption. [10–14] This allows to increase the performance of the solar cell. [1,15] This paper presents, on the one hand, a fabrication process and optimization of the optoelectronic parameters of a silver nanowire-based electrode, and on the other hand, its integration in an organic solar cell based on the recently developed PF2:PC70BM polymer-fullerene active layer. [16] This polymer is particularly interesting since it has demonstrated a very advantageous cost-effectiveness balance which make it a promising candidate for upscaling toward module fabrication. In addition, its large thickness (500 nm in this article), accessible via a significant length of

diffusion of the carriers, allows an ease of transposition to industrial processes. We will show here that despite its high thickness, and thus its high absorption, plasmonic electrodes are effective to boost its performance. A numerical study based on FDTD simulations on the impact of the plasmon resonance on the absorption of the active layer is also proposed.

## 2. Materials and methods

The fabrication of our devices required several materials purchased from approved suppliers. We used glass substrates (12x12mm$^2$) which are 1mm thick. They are first cleaned in an ultrasonic cleaner with acetone, ethanol, and isopropanol (10min for each solvent). A 10 min treatment with UV Ozone is done before deposition. The silver nanowires used as electrode are in the form of commercial solution purchased from CAMBRIOS Clear Ohm. They have a diameter between 31 and 40 nm and 25µm length. The electron transport layer (ETL) is based on zinc oxide nanoparticles (5nm diameter). They are in solution form purchased from Genes'Ink (Helios ETL Jet). The active layer is composed of a donor material (PF2:2-(4-{(3S,5S)-5-[(3,3-difluoropyrrolidin-1-yl)carbonyl]pyrrolidin-3-yl}piperazin-1-yl)pyrimidine) and a fullerene electron acceptor (PC70BM) (**Figure 1.c.**). [17] PC70BM ([6,6]-Phenyl-C71-butyric acid methyl ester) was purchased from American Dye Source. As hole transport layer (HTL), we use molybdenum trioxide ($MoO_3$) purchased from Sigma Aldrich. The top electrode is made of silver (99.99% purity) from Goodfellow.

The transparent silver nanowire electrode consists of three layers. The first layer is composed by ZnO nanoparticles. It has a thickness of 20 nm obtained by spin coating at a speed of 5000RPM, an acceleration of 1000RPM/s during 50s (**Figure 2.a.**). This layer allows a better adhesion of the silver nanowires on the substrate as it has been shown in our previous work [15]. The deposition of silver nanowires is done by spin coating with 2000RPM/s acceleration and 2000RPM speed over 60s. We then deposit 30nm of ZnO nanoparticles on top of the AgNWs in order to improve the surface roughness of our electrode. This last deposition is also done by spin coating. An annealing at 200°C for 10min is required after each step of the deposition.

The organic solar cell consists of a stack of thin films deposited in an inverted architecture (**Figure 1.a.**). **Figure 1.b.** shows that the relative energy levels of the different materials used is suitable for the collection of electrons on one side and holes on the other. For the reference device based on commercial ITO glass subtrates (purchased from Visiontek Limitd, UK), we first clean the TCO substrates with acetone, ethanol, isopropanol, and UV-Ozone treatment for 10 min. Then, we deposit 30nm of ZnONPs by spin coating (1000RPM/s, 4000RPM, 50s).

The film thus formed is annealed at 200°C for 10min. For both reference and AgNW-based devices, the PF2:PC70BM solution is prepared with chlorobenzene as solvent in the ratio 1:1.5, i.e., 7mg of PF2 and 10.5mg of PC70BM in 1 mL of solvent. The mixture is mixed few second under an ultra-sonic bath and then left under magnetic stirring at 80°C for 24h. It is heated to 105°C during 1.5h before deposition. For a better adhesion, the substrates are also heated to 105°C during 15min before deposition. As AgNWs can reach several tens of nanometers in roughness, this leads to a high probability of short-circuiting on conventional (100 nm) active layer thicknesses of organic solar cells. To solve this problem, we use PF2 as a donor material because it allows to reach important thickness of active layer. We then deposit 500 nm of PF2:PC70BM. The 500 nm thick PF2:PC70BM active layer is deposited by spin coating with the following parameters: step1: 600RPM, 500RPM/s, 20s; step2: 900RPM, 500RPM/s, 40s; step3: 2000RPM, 500RPM/s, 120s. [17] **Figure 1.d.** shows the absorption spectra of this active layer, conformed to the polymer. [17] The last step consists in evaporating 7nm of MoO3 and 100nm of Ag under secondary vacuum to complete the device (**Figure 1.a**). The solar cell with the ZAZ electrode is obtained by replacing the ITO electrode and the ZnO layer with the ZAZ one. The active area of the final device is 0.25cm$^2$.

Currente Voltage curves (J(V)) were obtained with solar simulator (K. H. Steuernagel Lichttechnik Gmbh) calibrated with Newport Oriel SN 10510-0021 and KEYTHLEY 2440. We use a UV-Visible spectrometer of Agilient Technologies model Carry 300 on the 200-800 nm range including an integrated sphere to determine the transmission spectrum of the electrode. We used air as reference sample making able to get the real transmission of the substrate/electrode (including the glass transmission) as it will be used in a realistic solar cell. The sheet resistance is determined with a 4-probe measurement equipment purchased from Lucas Labs. The morphological study of the different layers is done with an atomic force microscope (AFM Nano-Observer CSInstruments). ENLITECH QE-T equipment were used to measure the Incident Photo-Electron Conversion Efficiency (IPCE).

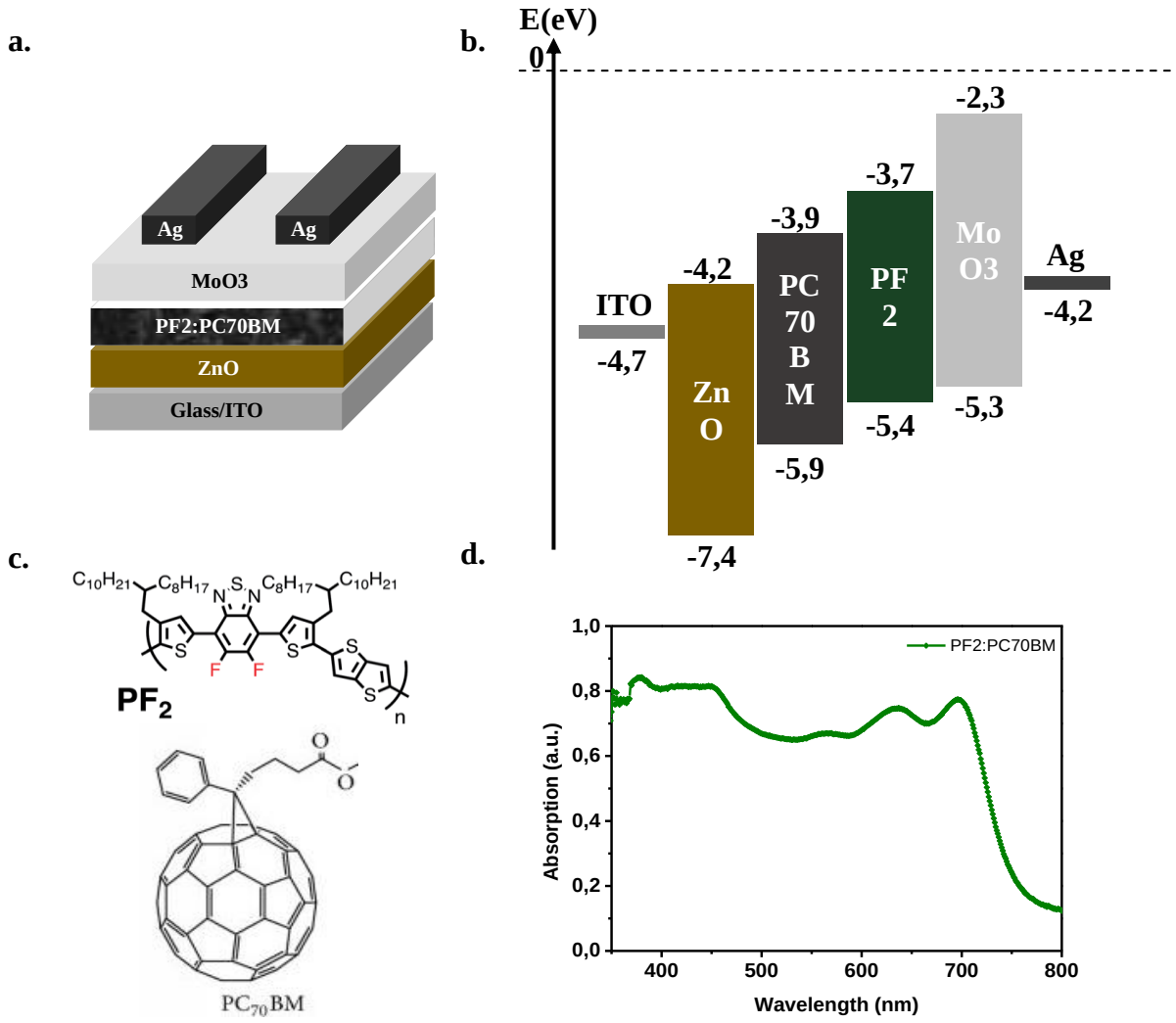


**Figure 1:** a. Schematic of the reference inverted organic solar cells considered in this work; b. energy level diagram of the materials[17] used in the organic solar cells; c. Molecular structure of PF2 and PC70BM; d. UV-Vis spectra of the active layer made by PF2:PC70BM.

3. ZAZ Electrode Optimization

Our study focuses on the two fundamental parameters associated with the development of transparent electrodes: conductivity and transmission. After the realization of the electrode, we study its optical, electrical, and morphological properties via dedicated characterization techniques. The AgNWs solution uses water as solvent. We varied the concentration of this solution from 30 to 7.5 mg/ml, and we noticed the variation of optical and electrical properties of the realized electrodes. The transmission increases strongly for low concentrations of AgNWs (**Figure 2.b**), in counterpart, the sheet resistance also increases strongly as we can see in **table 1**.

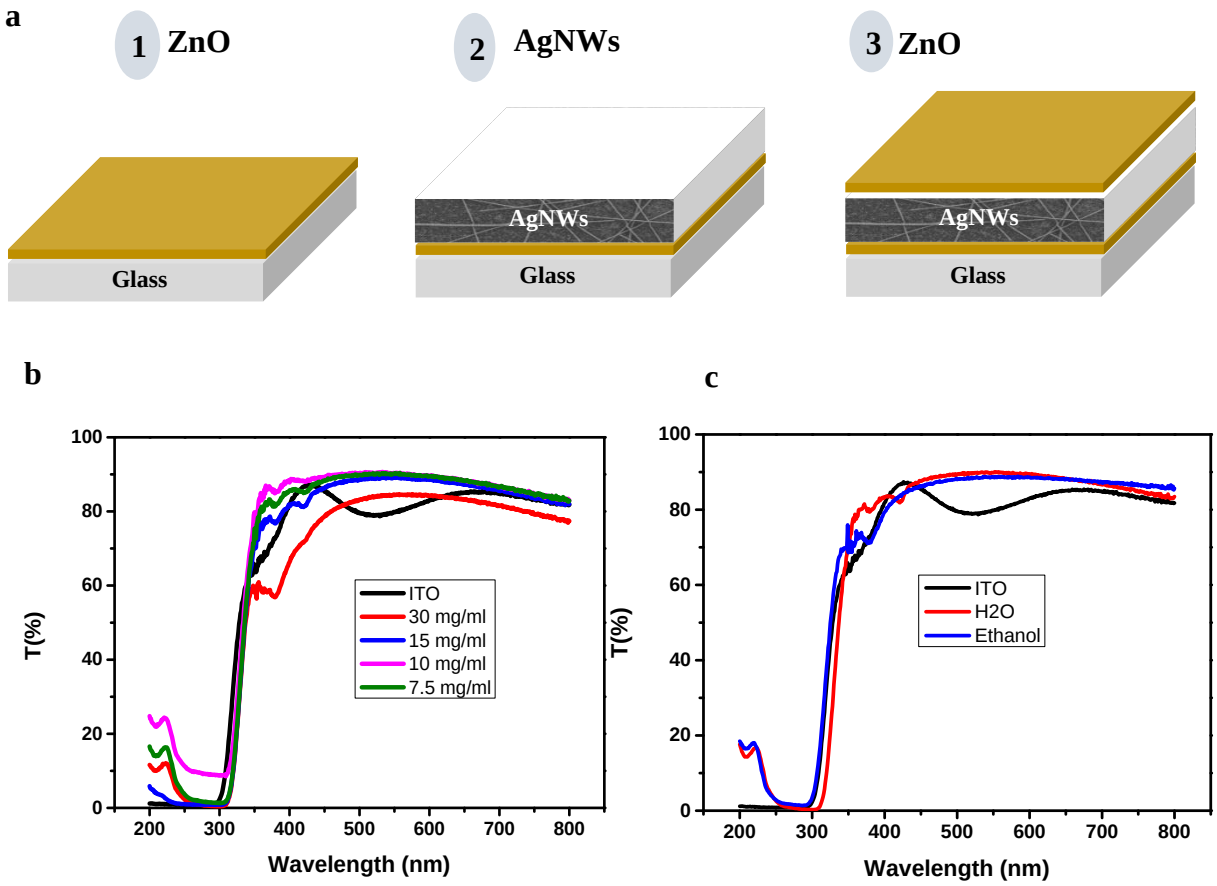


**Figure 2:** a. ZAZ electrode structure and deposition process; b. UV-Visible transmission spectra of ITO and ZAZ electrode for different concentration values (substrate included); c. UV-Visible transmission spectra of ZAZ electrode with H2O and Ethanol as solvent.

| Concentration ($mg.ml^{-1}$) | $R_{\square}$ ($\Omega/\square$) | T@350-800nm (%) | FoM |
|---|---|---|---|
| 30 | 19 | 78.5 | 77 |
| 15 | 52 | 85.3 | 43 |
| 10 | 180000 | 87 | - |
| 7.5 | 180000 | 87.7 | - |
| ITO | 7 | 81.7 | 254 |
| 15 (Ethanol) | 20 | 86.5 | 125 |

**Table 1:** Transmission, sheet resistance and figure of merit of ZAZ electrode with H2O solvent at different concentration, compared with ITO and ZAZ electrode with Ethanol solvent.

When the concentration of the solution is important, i.e. the density of the AgNWs is important, silver absorbs a part of the UV light and reflect a large part of the visible light. This allows to create a network of conductive AgNWs and decrease the optical transmission of the electrode. The challenge is to find the best trade-off between optical transmission and sheet resistance. A Figure of Merit (FoM), defined in the expression below, is used to quantify this trade-off. The total transmission *T* involved in the expression is the average value of the transmission calculated from 350 nm to 800 nm.

**Formula 1:** [18] $FoM = \frac{188,5}{R_{sq}(T^{-\frac{1}{2}}-1)}$ ; where $R_{sq}$ is the sheet resistance and T is the Transmission of the corresponding electrode.

For a concentration of 15 mg/ml, we have a very good transmission of the electrode (85.3%) but the sheet resistance appears high (52 Ω.sq-1). For OPV applications, the sheet resistance must be around 10 Ω.sq-1 in order to approach the performance of an ITO electrode. [19] In order to decrease the sheet resistance, we substituted water with ethanol as a solvent used in the AgNWs-based solution. [20] **Figure 2.c**, **Table 1** show the evolution of the electrode optoelectronic parameters as a function of experimental parameters. Silver nanowires are covered with polyvinylpyrrolidone (PVP) polymer when they are in solution to avoid a strong aggregation in the solution. This reduces the electrical conductivity of the final electrode, and so increase in the sheet resistance. The dissolution of PVP in ethanol [20] combined to a positive influence of the wettability of the solution on the substrate increased the transmission of the electrode and halved the sheet resistance. It improved the figure of merit of our electrode from 43 to 125 (**Table 1**). Improvements are still necessary to reach the performance of the reference ITO electrode whose figure of merit is 254.

In order to reach this objective, we performed a thermal annealing after the deposition of the electrode. Thermal annealing allows to melt the nanowires, to improve wires junctions by

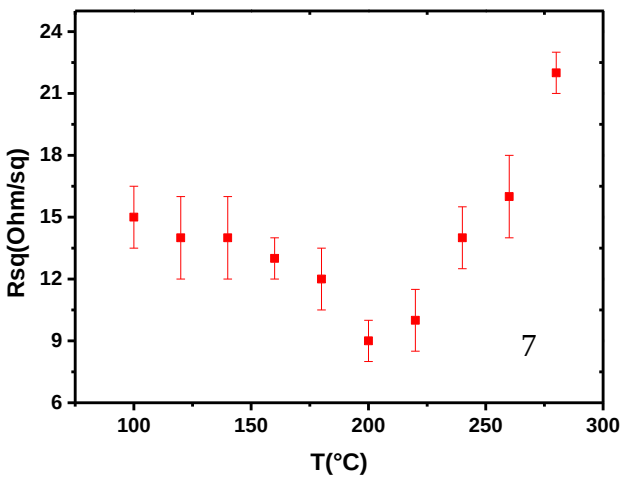

increasing the contact surface between each wire, to decreases the sheet resistance, until the temperature becomes too high so that silver agglomerates can form by fusion/coalescence, leading to of isolated nanoparticles. As can be seen in **Figure 3**, the optimum sheet resistance is obtained for an annealing at 200°C during 10min.

**Figure 3:** Sheet resistance variation with annealing temperature.

The last optimization concerns the intersections of AgNWs which contributes to a high roughness. These can create short circuits if their height is higher than that of the active layer as it can allow the anode to be in contact to the cathode. To solve this problem, we use a top layer of ZnO nanoparticles (ZnONPs) which will fill the gaps between wires and smooth the surface. Moreover, it is known that such sandwiched structure positively impacts the transmission spectrum of the whole electrode. [21] In **Figure 4** and **Table 2**, we show the evolution of the maximum height of the roughness profiles and RMS Roughness as a function of the top ZnONPs thickness of ZAZ electrode. **Table 3** summarizes the physical parameters and FoM of our different electrodes as a function of the main experimental parameters. The maximum height of these peaks (which is the highest peak monitored) and RMS roughness decreases as the thickness of the top layer of ZnO increases. On the other hand, the transmission decreases. The trade-off is obtained using 30nm for this top layer, which is consistent to the literature regarding the optimization of sandwiched electrodes. [22] Consequently, a very high FoM of 278 for the ZAZ electrode is achieved, which overperforms that of the reference ITO electrode.

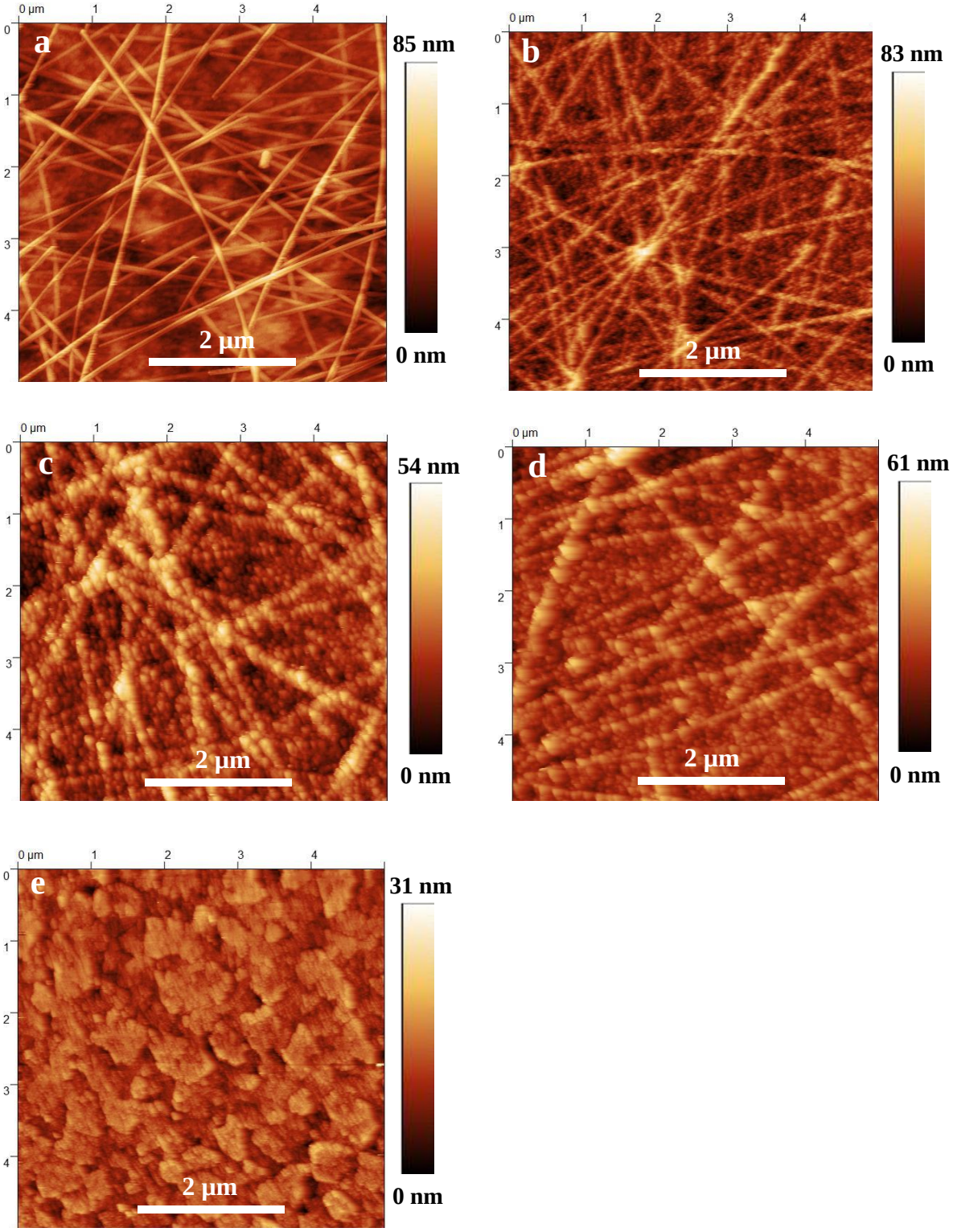


**Figure 4:** AFM images of **a.** ZnO(20nm)/AgNWs; **b.** ZnO(20nm)/AgNWS/ZnO(30nm); **c.** ZnO(20nm)/AgNWS/ZnO(60nm); **d.** ZnO(20nm)/AgNWS/ZnO(90nm); **e.** ITO

| | a. | b. | c. | d. | e. |
|---|---|---|---|---|---|
| **Max height of the roughness** | 68 ± 11nm | 24 ± 7 nm | 19 ± 3nm | 14 ± 2nm | 8 ± 2nm |
| **RMS Roughness** | 21 ± 5 nm | 15 ± 7 nm | 16 ± 4 nm | 13 ± 3 nm | 4 ± 2 nm |

**Table 2:** Maximum height of ZA, ZAZ and ITO roughness

| | Sample | ZnO | AgNWs (RPM) | ZnO | R□ (Ω/□) | T_350-800 nm (%) | FoM | Annealing (°C/10min) |
|---|---|---|---|---|---|---|---|---|
| b | ZAZ | 20 nm | 2000 | 30 nm | 9 | 86,5 | 278 | 200 |
| c | ZAZ | 20 nm | 2000 | 60 nm | 13 | 84,7 | 161 | 200 |
| d | ZAZ | 20 nm | 2000 | 90 nm | 24 | 82,4 | 77 | 200 |
| e | ITO | _ | _ | _ | 7 | 81,7 | 254 | - |

**Table 3:** Optimized parameters for ZAZ electrode deposition

4. Plasmonic resonance investigation in ZAZ electrodes

The plasmonic resonance related to AgNWs can contribute to the global performance of a solar cells. [23] To investigate this impact, we use a Finite Difference Time Domain modelling software (Lumerical FDTD) which solves Maxwell's equations in the time domain to evaluate the electrical field distribution around the 2D structure of our simplified electrode as described in **Figure 5.a**. We introduce periodic boundary conditions along the x direction and perfectly match layers (PML) along the y direction, which allows to absorb all the waves beyond the simulation area without reintroducing reflections. The incident light is in the form of two polychromatic plane waves along the z-axis and polarized with angles of 0 and 90° to best reflect the randomness of sunlight. To consider the optical phenomena related to our materials, we need to introduce their refractive indices. Thus, for AgNWs, we consider the optical indices from the book of Palik, [24] as for ZnONPs, we use the optical indices from the work of Li *et al.* [25] We set a thickness of 20 nm for the lower layer of ZnO and 30 nm for the upper layer of ZnO, which were the optimal thicknesses obtained in the experimental part. The diameter of AgNWs is 35 nm. The reflection, transmission and absorption of our simulated electrode is given in **Figure 5.b**. The plasmonic resonance is observed for a wavelength of 350 nm. This is coherent to the resonance of a silver nanoparticles surrounded with a ZnO layer. The plasmon is created at the silver/ZnO interface and lead to a generation of an intense electric field. Its repartition will be discussed later as it will directly impact the absorption of the surrounded material. [26] Simulations based on the Mie model suggest that an absorption enhancement can come from the Localised Surface Plasmon Resonance (LSPR)

and the effective scattering of light through silver nanostructures. [1,27] The FDTD simulation of the ZAZ electrode allowed us to visualize the electrical field distribution related to plasmonic resonance as a function of the wavelength. (**Figure 5.c & d**). A spatial extension of this electric field up to 20 nm away from ZnO interface is due to the plasmonic resonance and will reach the active layer placed here. Its absorption Q is proportional to the electric field squared as depict in the formula 2. More absorption means more electrons to collect and therefore a higher IPCE specifically in this spectral region.

Formula 2: $$Q(z,\lambda) = \alpha(\lambda)\frac{n_i}{n_0}\frac{|E(z)|^2}{|E_0|^2}$$ A

Moreover, the exaltation of the electric field appears to a large spectral area when it is integrated in the air area delimited in our modelling (**Figure 5.e**).

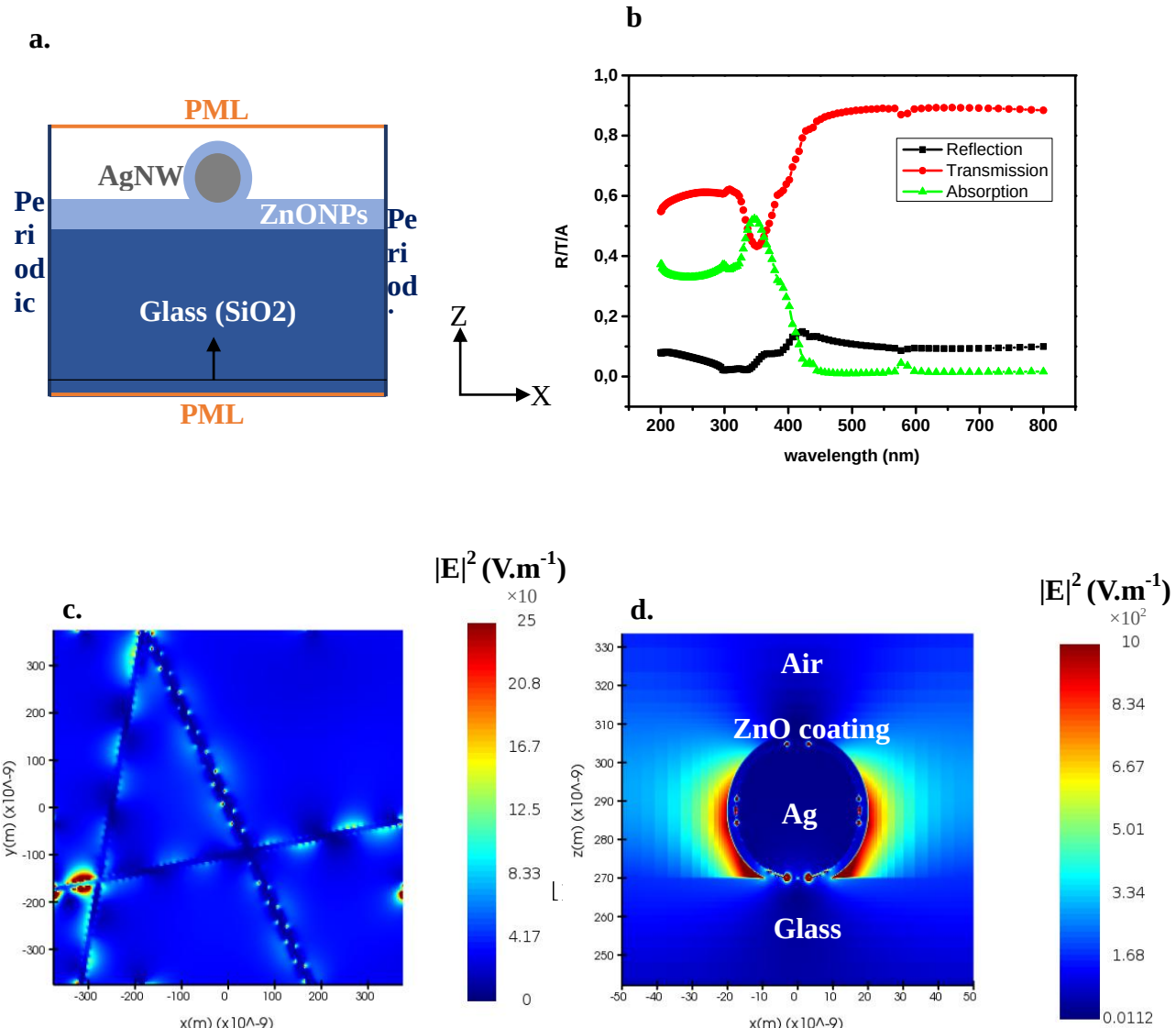

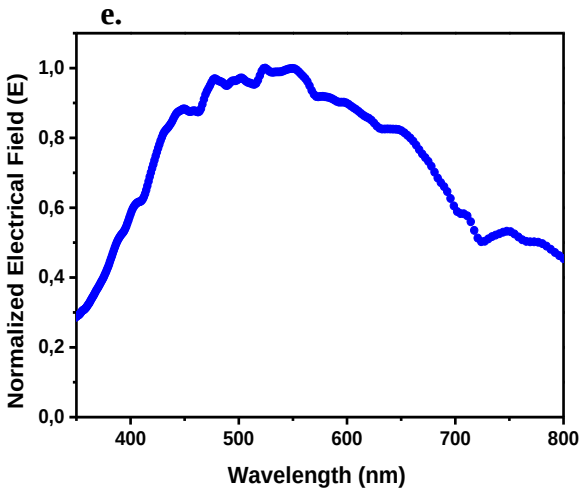


**Figure 5: a.** ZAZ Architecture simulated with Lumerical FDTD Solution; **b.** Related Reflection, Transmission and Absorption; ZAZ electrode electrical field simulated at 454 nm **c.** top view; **d.** cross section view; e. Normalized Electrical Field of Simulated ZAZ electrode.

## 5. OPV Performance

In presence of AgNWs, we observe an increase in the active layer absorption (**Figure 6.a**). Since the thickness of the active layer remains unchanged and thick (500 nm), the increase in absorption is significative to a stronger transmission of the silver nanowires than of the ITO and a possible scattering of light generated by the surface of the nanowires. The transmission of ZAZ being higher than that of ITO except between 400 and 450 nm (**Figure 2.c**). The absorption goes from about 80% to 90% (difference of 10%) up to a wavelength of 480 nm when the nanowires are used instead of the ITO. This difference in absorption increases from 10% to 20% beyond this wavelength. In the first spectral region, the nanowires absorb light due to the plasmon effect. Plasmonic resonance allow to compensate this by an increase of the active layer absorption, even if the resonance is limited to a few tens of manometers inside the active layer of 500 nm thick. [1,28] On 35 nm layers (**Figure 6.b**) we can easily see the impact of the plasmonic resonance on the absorption, from 350 nm to 450 nm. Indeed, we observe an increase in the absorption with ZAZ due to the plasmonic effect as we have demonstrated in our FDTD simulations (**Figure 5**). The plasmon is present in this structure and visible only

with a thin active layer. Thus, **figure 6.a** does not make it appear clearly because the favourable transmission of the nanowires has increased the other spectral regions not shaded by the nanowires, mixing the beneficial effects of this electrode. The plasmonic gain and the highest transmission of the ZAZ induce an increase of the IPCE (**Figure 6.c**) in the full visible spectrum. Plasmon effect related to the silver nanowires improve the area between 350 nm and 450 nm. The photogenerated current is proportional to the absorption and is a consequence of an increase of the IPCE at the plasmonic resonance and beyond (**Figure 6.c**) This result is consistent with the current density / voltage curves (IV) (**Figure 6.d**) and lead to an improvement of the Jsc of 39 %, and therefore and improvement of the power conversion efficiency of the cells from 6.08% (ITO) to 8.13% (ZAZ) (**table 4**). To obtain IV measurements, we calculated our missmatch factor on the reference devices integrating an ITO electrode. It is interesting to see that the currents obtained by IPCE or IV on these solar cells are consistent (14.09 mA/cm² vs 14.51 mA/cm²), but a difference exists when this same missmatch is used on devices integrating silver nanowires (17.33 mA/cm² vs 20.25 mA/cm²). Indeed, the plasmon modifying the absorption in the blue area of the spectrum of the solar cell, the latter has a different sensitivity. It is then possible to overestimate the currents under solar simulator. The improvement in efficiencies is still high with a value of 20% when the missmatch factor is considered.

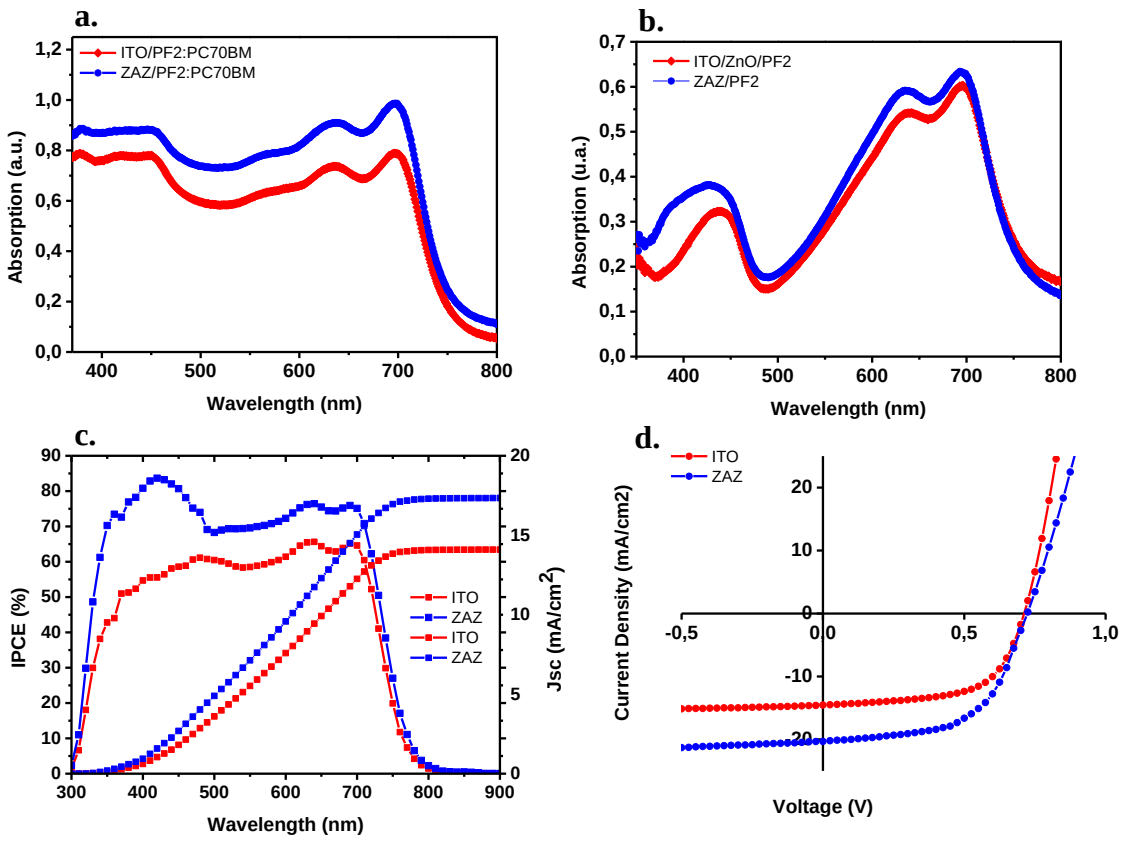


**Figure 6: a.** Absorption spectra of the active layer with ITO and ZAZ electrode; **b.** Absorption spectra of a thin layer of 35 nm PF2 on ZAZ and ITO/ZnO; **c.** IPCE Spectra oh the organic solar cells with ITO and ZAZ electrode and associated calculated current under AM15G (ZAZ: 17.33 mA/cm²; ITO: 14.09 mA/cm².); **d.** J(V) curves of the organic solar cells with ITO and ZAZ electrode; **e.** PL spectra of PF2 on ITO and ZAZ electrode; **f.** TRPL spectra of PF2 on ITO and ZAZ electrode. Excitation wavelength is 377 nm for PL and TRPL, we also did a deconvolution that include equipment response.

| Cathode | Voc(V) | Jsc(mA/cm2) | FF | □(%) | Rs (Ω) | Rsh (Ω) |
|---|---|---|---|---|---|---|
| ITO | 0.687 | 14.51 | 0.61 | 6.08 | 28 | 1978 |
| ZAZ | 0.705 | 20.25 | 0.57 | 8.13 | 31 | 1433 |

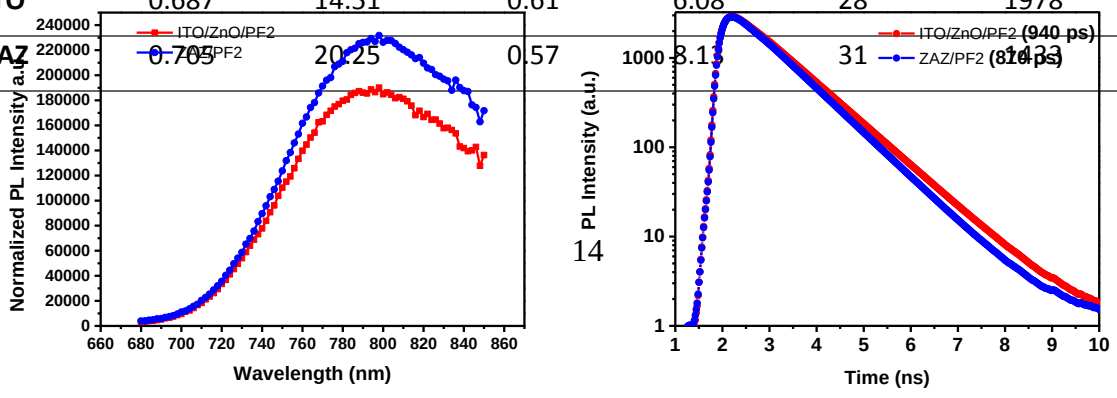

**Table 4:** Device parameters with ZAZ and ITO electrode under AM 1.5 solar illumination with Intensity of 100 mW/cm$^2$.

To better understand the impact of plasmon resonance on our solar cells, we performed photoluminescence spectroscopy (**Figure 6.e.**). Using 377 nm excitation, we observe a considerable increase in PF2 emission in the presence of ZAZ compared to ITO, this is due to the plasmon exaltation in the vicinity of AgNWs as we manage to excite AgNWs close to their resonances. The density of photogenerated excitons increases caused by the strong excitation and trapping of light. [29–31] Time-Resolved Photoluminescence (TRPL) allowed us to determine the exciton lifetime as can be seen in **Figure 6.f.** In case of ZAZ involvement, the exciton lifetime is shorter. This trend, however slight, is nevertheless systematically observed. The plasmon coupling with the exciton induces a fast charge separation because the localized electrical field around the AgNWs contributes to the charge separation in the exciton, hence the shorter lifetime. [32] Chen *et al.* [30] and Wu *et al.* [31] explained this phenomenon by a strong "plasmon-exciton" coupling giving rise to a charge transfer and a modification of the properties of the generated excitons. The photophysical process is interpreted via the concept of "hot electron" to overcome the initial Coulomb potential. [33,34]

## 6. Conclusion

To conclude, we developed and studied a AgNWs based electrode easily processed from solution, and we demonstrated the relevance of using a sandwich structure based on lower and upper ZnO layers, which improve its optoelectronic performance compared to an ITO reference. The enhancement of both electrical conductivity and optical transmission by diluting the AgNWs solution with ethanol and applying a post-deposition thermal annealing, allow the achievement of improved photovoltaic performance, when applied to organic solar cells. The interaction of light with silver induces a phenomenon better known as plasmon resonance. A simulation of the ZAZ electrode on Lumerical FDTD allowed us to visualize the spatial and spectral distribution of the electrical field generated by the AgNWs, which extends to the visible wavelengths, explaining the increase of the photogenerated current observed in the devices under solar illumination. Through photoluminescence spectroscopy, we also

observed a shorter exciton lifetime in the presence of AgNWs compared to the reference ITO/ZnO substrate. We highlight that if the IPCE is not high by default on a non-plasmonic electrode, despite a high active layer thickness, it is possible to boost it thanks to silver nanowires. All these phenomena allowed us to increase the efficiency and the current by 20% of our solar cell compared to the solar cell realized with the ITO electrode. AgNWs based electrodes offer a valuable alternative to ITO due to their superior performance. They can be used in various fields such as light detection and emission.

References:

[1] L. Feng, M. Niu, Z. Wen, X. Hao, *Polymers* **2018**, *10*, 123.
[2] F.C. Krebs, M. Jørgensen, K. Norrman, O. Hagemann, J. Alstrup, T.D. Nielsen, J. Fyenbo, K. Larsen, J. Kristensen, *Sol. Energy Mater. Sol. Cells* **2009**, *93*, 422–441.
[3] NREL, Best Research-Cell Efficiency Chart, https://www.nrel.gov/pv/cell-efficiency.html, accessed: May, **2022**.
[4] Z. Zheng, J. Wang, P. Bi, J. Ren, Y. Wang, Y. Yang, X. Liu, S. Zhang, J. Hou, *Joule* **2022**, *6*, 171–184.
[5] A.C. Mayer, S.R. Scully, B.E. Hardin, M.W. Rowell, M.D. McGehee, *Mater. Today* **2007**, *10*, 28–33.
[6] S.M. Falke, C.A. Rozzi, D. Brida, M. Maiuri, M. Amato, E. Sommer, A. De Sio, A. Rubio, G. Cerullo, E. Molinari, C. Lienau, *Science* **2014**, *344*, 1001–1005.
[7] K. Ellmer, *Nat. Photonics* **2012,** *6*, 809–817.
[8] P. Kou, L. Yang, C. Chang, S. He, *Sci. Rep.* **2017**, *7*, 42052.
[9] M. Raïssi, S. Vedraine, R. Garuz, T. Trigaud, B. Ratier, *Sol. Energy Mater. Sol. Cells* **2017**, *160*, 494–502.
[10] D.H. Wang, D.Y. Kim, K.W. Choi, J.H. Seo, S.H. Im, J.H. Park, O.O. Park, A.J. Heeger, *Angew. Chem. Int. Ed.* **2011**, *50*, 5519–5523.
[11] H.I. Park, S. Lee, J.M. Lee, S.A. Nam, T. Jeon, S.W. Han, S.O. Kim, *ACS Nano* **2014**, *8*, 10305–10312.
[12] S. Vedraine, P. Torchio, A. Merlen, J. Bagierek, F. Flory, A. Sangar, L. Escoubas, *Sol. Energy Mater. Sol. Cells* **2012**, *102*, 31–35.
[13] D. Kozanoglu, D.H. Apaydin, A. Cirpan, E.N. Esenturk, *Org. Electron.* **2013**, *14*, 1720–1727.
[14] C.-M. Liu, C.-M. Chen, Y.-W. Su, S.-M. Wang, K.-H. Wei, *Org. Electron.* **2013**, *14*, 2476–2483.
[15] M. Chalh, S. Vedraine, B. Lucas, B. Ratier, *Sol. Energy Mater. Sol. Cells* **2016**, *152*, 34–41.
[16] O. Ibraikulov, J. Wang, K. Narayanaswamy, B. Heinrich, S. Méry, M. Kohlstädt, U. Würfel, S. Ferry, N. Leclerc, T. Heiser, P. Lévêque, *Sol. RRL* **2019**, *3*.
[17] O.A. Ibraikulov, C. Ngov, P. Chávez, I. Bulut, B. Heinrich, O. Boyron, K.L. Gerasimov, D.A. Ivanov, S. Swaraj, S. Méry, N. Leclerc, P. Lévêque, T. Heiser, *J. Mater. Chem.* **2018**, *A 6*, 12038–12045.
[18] D. Kumar, V. Stoichkov, E. Brousseau, G.C. Smith, J. Kettle, *rsc.li/nanoscale* **2019**, *11*.
[19] Y. Sun, M. Chang, L. Meng, X. Wan, H. Gao, Y. Zhang, K. Zhao, Z. Sun, C. Li, S. Liu, H. Wang, J. Liang, Y. Chen, *Nat. Electron.* **2019**, *2*, 513–520.
[20] J. Wang, J. Jiu, T. Araki, M. Nogi, T. Sugahara, S. Nagao, H. Koga, P. He, K. Suganuma, *Nano-Micro Lett.* **2015**, *7*, 51–58.
[21] S. Vedraine, A. El Hajj, P. Torchio, B. Lucas, *Org. Electron.* **2013**, *14*, 1122–1129.
[22] D.-T. Nguyen, S. Vedraine, L. Cattin, P. Torchio, M. Morsli, F. Flory, J.C. Bernède, *J. Appl. Phys.* **2012**, *112*, 063505.
[23] M. Piralaee, Z. Ebrahimpour, A. Asgari, *Curr. Appl. Phys.* **2020**, *20*, 531–537.
[24] E.D. Palik, *Handbook of Optical Constants of Solids*, Academic Press, **1998**.
[25] Q.H. Li, D. Zhu, W. Liu, Y. Liu, X.C. *Ma, Appl. Surf. Sci.* **2008**, *254* 2922–2926.
[26] S. Vedraine, P. Torchio, D. Duché, F. Flory, J.-J. Simon, J. Le Rouzo, L. Escoubas, *Sol. Energy Mater. Sol. Cells* **2011**, *95*, S57–S64.
[27] Y.-S. Hsiao, S. Charan, F.-Y. Wu, F.-C. Chien, C.-W. Chu, P. Chen, F.-C. Chen, *J. Phys. Chem.* **2012**, *C 116*, 20731–20737.
[28] S.-W. Baek, J. Noh, C.-H. Lee, B. Kim, M.-K. Seo, J.-Y. Lee, *Sci. Rep.* **2013**, *3*,1726.
[29] Y. Yang, J. Qing, J. Ou, X. Lin, Z. Yuan, D. Yu, X. Zhou, X. Chen, *Sol. Energy* **2015**, *122*, 231–238.

[30] T.Z. Oo, N. Mathews, G. Xing, B. Wu, B. Xing, L.H. Wong, T.C. Sum, S.G. Mhaisalkar, *J. Phys. Chem.* **2012**, *C 116*, 6453–6458.
[31] C.-S. Kao, F.-C. Chen, C.-W. Liao, M.H. Huang, C.-S. Hsu, *Appl. Phys. Lett.* **2012,** *101*, 193902.
[32] K. Okamoto, I. Niki, A. Shvartser, Y. Narukawa, T. Mukai, A. Scherer, *Nat. Mater.* **2004**, *3*, 601–605.
[33] F.-C. Chen, J.-L. Wu, C.-L. Lee, Y. Hong, C.-H. Kuo, M.H. Huang, *Appl. Phys. Lett.* **2009**, *95*, 013305.
[34] J.-L. Wu, F.-C. Chen, Y.-S. Hsiao, F.-C. Chien, P. Chen, C.-H. Kuo, M.H. Huang, C.-S. Hsu, *ACS Nano* **2011**, *5*, 959–967.

I. Ibrahim Zamkoye, J. Bouclé, N. Leclerc, B. Lucas, S. Vedraine

**Silver Nanowire Electrodes Integrated in Organic Solar Cells with Thick Active Layer Based on a Low-Cost Donor Polymer**

ToC figure ((Please choose one size: 55 mm broad × 50 mm high **or** 110 mm broad × 20 mm high. Please do not use any other dimensions))